Journal of Turbulence
Volume 6, No. 30, 2005

Taylor & Francis
Taylor & Francis Group

Experimental study of velocity boundary layer near a rough conducting surface in turbulent natural convection

X.-L. QIU†, K.-Q. XIA*† and P. TONG‡

†Department of Physics, The Chinese University of Hong Kong, Shatin, Hong Kong, China
‡Department of Physics, Hong Kong University of Science and Technology, Clear Water Bay, Kowloon, Hong Kong, China

Dual-beam intensity cross-correlation spectroscopy is used to measure the viscous boundary layer over a rough conducting surface in turbulent convection in water. It is found that the velocity boundary layer near the rough surface can be characterized by three quantities: the maximum velocity v_m, the shear rate γ_v and the total boundary layer thickness $d + \delta_v$; all of them obey power laws of Rayleigh number Ra. The maximum velocity v_m is located outside the rough surface and its numerical value remains the same as that in the smooth cell. The Ra-dependence of $d + \delta_v$ is found to be the same as that in the smooth cell, but the power-law amplitude is increased by a factor close to 2. Because of the formation of small eddies inside the roughening grooves, the measured γ_v is reduced considerably in the groove region. It is also found that the Nusselt number $Nu \sim Ra^{0.35}$, which is larger in both magnitude and scaling exponent as compared to the smooth case.

1. Introduction

In recent years, there has been a growing interest to study turbulent natural convection over rough conducting surfaces both experimentally [1–4] and theoretically [5]. These studies are motivated partially by the desire for a more fundamental understanding of the heat transport in high-Rayleigh-number turbulent natural convection [6]. They are also relevant to many practical applications, because most free convections occurring in nature are over surfaces of corrugated topology (such as oceanic and atmospheric convections). It has been shown [2, 4] that the heat transport in the convection cell with rough upper and lower conducting surfaces is increased considerably when compared with that in the smooth cell. Flow visualization and near-wall temperature measurements revealed that the interaction between the large-scale horizontal flow and the ordered rough surface creates a secondary flow (eddies) in the groove region. The secondary flow together with the large-scale circulation enhance the detachment of the thermal boundary layer from the tip of the rough elements. These extra thermal plumes are believed to be responsible for the enhanced heat transport in the rough cell.

While systematic temperature measurements [1, 2, 4] have been conducted to study the emission dynamics of the thermal plumes near the rough surface, direct velocity measurements have not been made in the rough convection cell. The lack of the velocity information prevents us from answering some important questions that are related directly to the physical

*Corresponding author.

Journal of Turbulence
ISSN: 1468-5248 (online only)
http://www.tandf.co.uk/journals
DOI: 10.1080/14685240500460733

understanding of convective turbulence in general and turbulent heat transport in particular. These questions include: How does the surface roughness modify the velocity boundary layer in turbulent natural convection? Do the thermal plumes that erupt from the upper and lower thermal boundary layers and the large-scale circulation that spans the height of the cell change in the rough cell? These two coherent structures have been found to coexist in the smooth cell [7, 8]. Clearly, a systematic study of the velocity field near the rough surface will provide further understanding of the heat transport in turbulent natural convection.

Previous studies of rough-wall velocity boundary layers in wind tunnels and other open flow systems have shown [9] that the surface roughness usually does not perturb the turbulent bulk region very much and its effect is confined mainly in the near-wall region. The velocity boundary layer in turbulent natural convection, however, differs greatly from those in open flow systems. Because the convection experiment is conducted in a closed cell, the disturbances produced by the rough boundaries are inevitably mixed into the turbulent bulk region. Furthermore, the thermal plumes emitted from the conducting surfaces introduce strong perturbations to the velocity boundary layers [10]. To study the interaction between the velocity and thermal boundary layers, it becomes important to alter the boundary conditions and see how the surface roughness affects the velocity and thermal boundary layers, respectively.

In this paper, we report the first experimental study of the velocity boundary layer near a rough conducting surface in turbulent natural convection. A newly developed technique of dual-beam incoherent cross-correlation spectroscopy [11] is used to measure the velocity profiles near the rough surface and their Rayleigh-number dependence. To facilitate the velocity measurements, we use water as the convecting fluid and the Rayleigh number is varied in the range $10^8 < Ra < 10^{10}$.

2. Experimental setup and method

Figure 1 shows a schematic diagram of the convection cell used in the experiment. The upper and lower plates are made of copper and their surfaces are electroplated with a thin layer of gold. Copper plates are chosen because of their good thermal conductivity, and the thin gold layer is used to prevent oxidation. The sidewall of the cell is made of a transparent Plexiglas tube, which can admit the incident laser light and transmit the scattered light. The diameter and the height of the cell are 19 and 19.6 cm, respectively. The aspect ratio of the cell is thus near unity. The two plates and the Plexiglas tube are held together by six thin posts. The post consists of two stainless steel rods separated by a Teflon rod to prevent heat leakage. The upper and lower rough surfaces have woven V-shaped grooves on them. The grooves have a vertex angle of 90°, and their spacing is such that a square lattice of pyramids is formed on the surface. The pyramid height (roughness height) is $k = 8$ mm and the spacing between the grooves is $2k$. To compare the velocity measurements, we also use another pair of rough surfaces that have the same surface structure but the roughness height is $k = 3$ mm. As shown in figure 1(b), the z-coordinate measures the vertical distance from the bottom of the groove and the x-axis points to the direction of the horizontal flow near the surface.

The temperature of the upper plate is regulated by passing cold water through a cooling chamber fitted on top of the plate. The lower plate is heated uniformly at a constant rate with an embedded film heater. The temperature of each plate is measured by two thermistors embedded in the plate; one is placed at the centre of the plate and the other is 5 cm away from the centre. The measured relative temperature difference between the two thermistors is found to be less than 1% for both plates at all Rayleigh numbers, indicating that the temperature across each plate is uniform. The control parameter in the experiment is the Rayleigh number

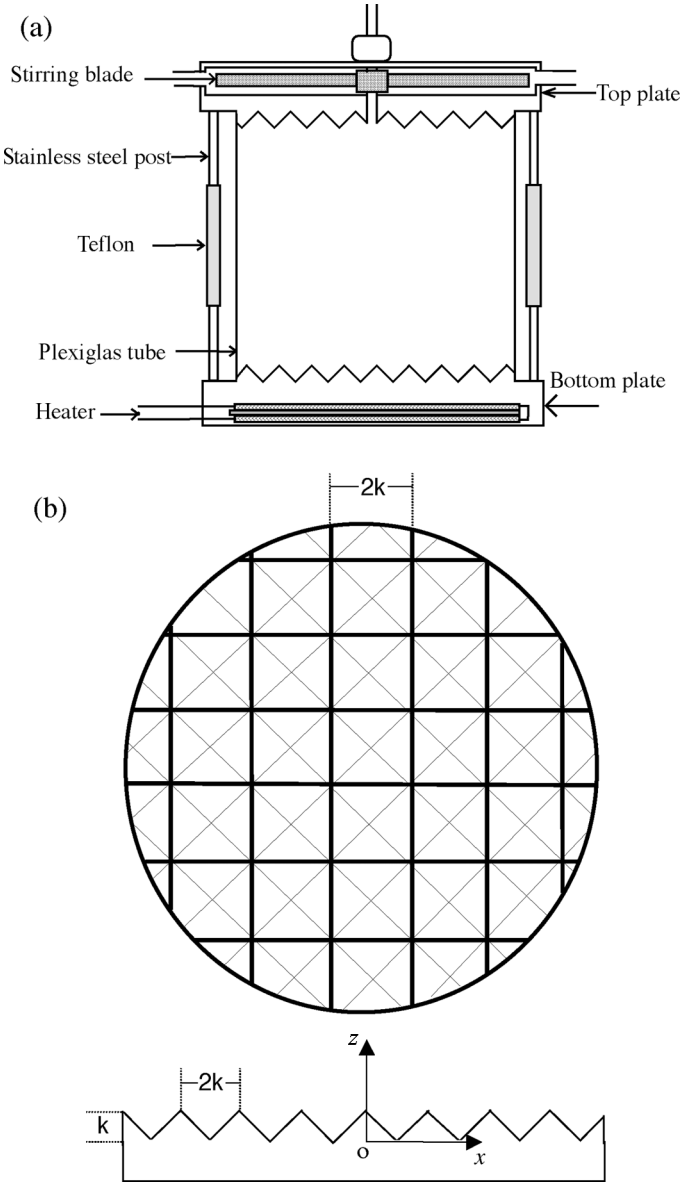

Figure 1. (a) Sketch of the convection cell with rough upper and lower conducting plates. (b) Top and side views of the rough conducting plate. The coordinate system is shown with the x-axis being the direction of the large-scale circulation.

$Ra = \alpha g L^3 \Delta T/(\nu\kappa)$, where g is the gravitational acceleration, L is the cell height, ΔT is the temperature difference between the two plates, and α, ν and κ are, respectively, the thermal expansion coefficient, the kinematic viscosity, and the thermal diffusivity of water, which is used as the convecting fluid. In the experiment, we maintain the temperature of the bulk fluid at 23°C and vary the temperature difference ΔT. In this way, the Prandtl number $Pr = \nu/\kappa$ is fixed ($Pr \simeq 7$) and all the fluid properties are determined based on the bulk fluid temperature.

The velocity measurements are carried out using the technique of dual-beam incoherent cross-correlation spectroscopy. Details about the technique have been described elsewhere

[11, 12], and here we mention only some key points. In the experiment, two parallel laser beams with a known separation ℓ are shone through the convecting fluid. The two beams are the blue and green lights from an argon–ion laser operated under the multiline mode. The fluid is seeded with nearly buoyant polymer latex spheres of 0.95 μm in diameter. The velocity of the seed particles is determined by measuring the time required for the particles to cross the two parallel beams in succession. Experimentally, this transit time is obtained from the intensity cross-correlation function

$$g_c(t) = \frac{\langle I_b(t')I_g(t'+t)\rangle}{\langle I_b(t')\rangle\langle I_g(t')\rangle} = 1 + \beta G_c(t), \tag{1}$$

where t is the delay time and the angular brackets represent the time average over t'. In the above, β (≤ 1) is an instrumental constant, $I_b(t)$ and $I_g(t)$ are the scattered light intensities from the blue and green beams, respectively. Because there is no phase coherence between $I_b(t)$ and $I_g(t)$, $g_c(t)$ is sensitive only to the scattering amplitude fluctuations produced by the seed particles moving in and out of the laser beams.

For a uniform flow with a velocity v in the direction perpendicular to the laser beams, $G_c(t)$ in equation (1) has the form [11]

$$G_c(t) = \frac{\mathrm{e}^{-(vt-\ell)^2/r_0^2}}{N}, \tag{2}$$

where r_0 is the radius of the laser beam, ℓ is the separation between the two laser beams, and N is the average number of the particles in the scattering volume. For a turbulent flow $G_c(t)$ becomes [13]

$$G_c(t) = \frac{1}{N}\int \mathrm{d}v\, P(v) \exp\left(-(vt-\ell)^2/r_0^2\right) = \frac{\exp\left(-(v_0t-\ell)^2/[r_0^2+2(\sigma t)^2]\right)}{N\sqrt{1+2(\sigma t/r_0)^2}}. \tag{3}$$

In the above, the probability density function (PDF) $P(v)$ of the local velocity v has been assumed to be of a Gaussian form with v_0 being the mean velocity and σ the standard deviation. It has been found in previous experiments that $P(v)$ is Gaussian-like even in the boundary layer region [13–15]. It has also been estimated [15] that the boundary layer thickness-based shear Reynolds number reached in convection experiments of comparable values of *Ra* and *Pr* is about 200 at most, whereas the critical value for boundary layer instability is 420 [16]. This suggests that in convection experiments conducted in the present range of *Ra* and *Pr* the boundary layer is essentially laminar and intermittency does not contribute significantly to velocities measured in the boundary layer region.

Figure 2 shows a schematic diagram of the experimental setup. The argon–ion laser (Coherent Innova-300) is under the multiline operation with a wavelength range from 457.9 to 514.5 nm. The prism is positioned in such a way that the exit point of the laser beams is at the focal point of the achromatic lens L1. This ensures that the two laser beams of different colours become parallel after passing through L1. The distance between L1 and the convection cell is adjusted so that the two parallel beams are focused separately at the cell centre. To determine the beam separation ℓ and radius r_0, we place a small flow cell at the centre of a large cylindrical cell filled with water. The cylindrical cell is made of the same transparent Plexiglas tube and has the same dimension as that of the convection cell. The flow cell is a short piece of rectangular glass tubing (1.0 mm $\times$ 9.18 mm in cross section) together with a circulating loop. A small pump is used to generate a laminar flow and its speed at the cell centre is calibrated by the known flow rate. The laminar nature of the flow is verified by the measured Poiseuille velocity profile in the flow cell. The measured $G_c(t)$ is found to be well fitted by equation (2) with $\ell = 0.30$ mm and $r_0 = 0.06$ mm. The achromatic lens L2 situated normal to the incident laser beams projects the image of the scattered beams inside the cell onto an adjustable slit

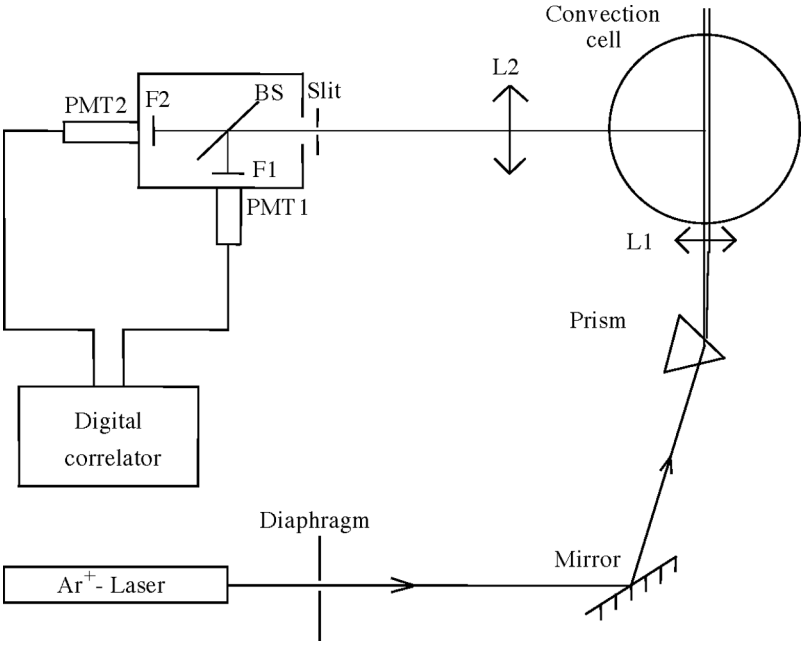

Figure 2. Schematic diagram of the experimental setup. L1, L2: lenses; BS: beam splitter; F1, F2: interference filters; PMT1, PMT2: photomultiplier tubes.

with 1:1 magnification. The slit is so positioned that only the central portion of the scattered beams are viewed by the two photomultiplier tubes (PMT1 and PMT2). The two photomultiplier tubes are mounted at right angle on a cubic box, and the beam splitter BS at the center of the box has a reflection-to-transmission ratio of 50/50. The two interference filters (F1 and F2) have a bandwidth of 1 nm centred at 488.0 and 514.5 nm, respectively. The pulse trains from PMT1 and PMT2 are fed to a digital correlator (ALV-5000), whose output gives $g_c(t)$.

The whole convection cell sits on a rotation-translation stage, which can travel 20 cm in the vertical direction with an accuracy of 0.01 mm. With the translation stage, we can adjust the vertical distance between the laser beams and the lower surface of the cell and measure the velocity profile $v(z)$ along the central vertical axis (z-axis) of the cell. We can also rotate the cell about the z-axis and change the azimuthal orientation of the cell relative to the incident laser beams.

A unique feature of the dual-beam method is that it can measure the local velocity near the thermal boundary layer, in which large temperature fluctuations produce strong fluctuations of the fluid refractive index. These fluctuations may cause the two focusing laser beams used in laser Doppler velocimetry (LDV) to wander and defocus in the fluid. This corruption of laser beam properties severely limits the application of LDV near the rough conducting surface. In contrast to LDV, the dual-beam method uses two parallel beams rather than two focusing beams, and therefore avoids the defocusing problem near the thermal boundary layer. With the receiving optics shown in figure 2, the measurement of $G_c(t)$ is not affected by the small beam wandering in the convecting fluid (up to 1 mm in amplitude). This beam wandering occurs mainly in the temperature gradient (vertical) direction and its amplitude is smaller than the thermal boundary layer thickness, which is less than 1 mm in our working range of *Ra*.

Another advantage of the dual-beam method is that it can distinguish the flow direction (v or $-$v) by simultaneously measuring the 'green-cross-blue' (GCB) correlation function

$\langle I_g(t')I_b(t'+t)\rangle/\langle I_b(t')\rangle\langle I_g(t')\rangle$, in which the measured $I_b(t)$ is delayed relative to $I_g(t)$, and the 'blue-cross-green' (BCG) correlation function $\langle I_b(t')I_g(t'+t)\rangle/\langle I_b(t')\rangle\langle I_g(t')\rangle$. If a seed particle first passes the green and then the blue beams, delaying $I_b(t)$ with a time interval equal to that for the particle to cross the two laser beams will give a nonzero intensity product, $\langle I_g(t')I_b(t'+t)\rangle$. For other delay times the average of the intensity product is zero, since the delay time does not match the beam crossing time. Obviously, for the same flow direction, the BCG does not have a peak because $I_g(t)$ is delayed in the wrong direction.

3. Results and discussion

3.1 *Velocity profiles near the rough surface*

The digital correlator used in our experiment can produce simultaneously two time-crosscorrelation functions using its two signal input channels A and B, one with A delayed relative to B and the other vice versa. All our measurements are made with the correlator operated under this 'dual-cross' mode. Figure 3 shows the GCB (circles) and BCG (squares) cross-correlation functions measured simultaneously at $Ra = 4.3 \times 10^9$ and at $z = 7.9$ mm (along the central vertical axis). In this measurement the two beams are oriented such that only the horizontal velocity v_h is measured. To ensure that we measure the speed of the large-scale circulation (LSC), the convection cell is rotated about the z-axis with respect to the incident laser beams so that a maximum value of v_h is obtained, which also indicates that the laser beams are now perpendicular to the azimuthal plane of the LSC. It is seen from figure 3 that the measured GCB is a singly peaked function, whereas the BCG is a simple decaying function without the peak. The decay of the BCG is caused by the velocity fluctuations across the beam radius r_0 (see equation (3)). The solid line in figure 3 shows the fit to equation (3) with $v_0 = 1.67$ cm/s and $\sigma = 0.39$ cm/s. It is found that the measured $G_c(t)$ at different values of z and Ra can all be fitted to equation (3). Figure 3 thus suggests that v_h is essentially uni-directional near the rough surface and its PDF $P(v_h)$ can be described by a Gaussian function. We also measured the vertical velocity v_v near the boundary. Within the sensitivity

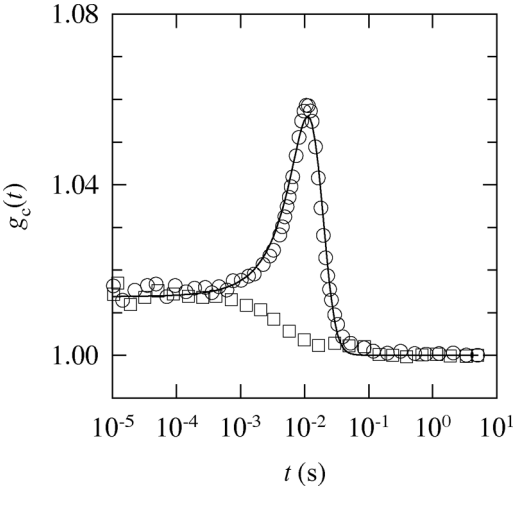

Figure 3. Measured 'green cross blue' (circles) and 'blue cross green' (squares) correlation functions $g_c(t)$ in the rough cell with $k = 8$ mm. The measurements are made at $z = 7.9$ mm and $Ra = 4.3 \times 10^9$. The solid curve is a fit by equation (3).

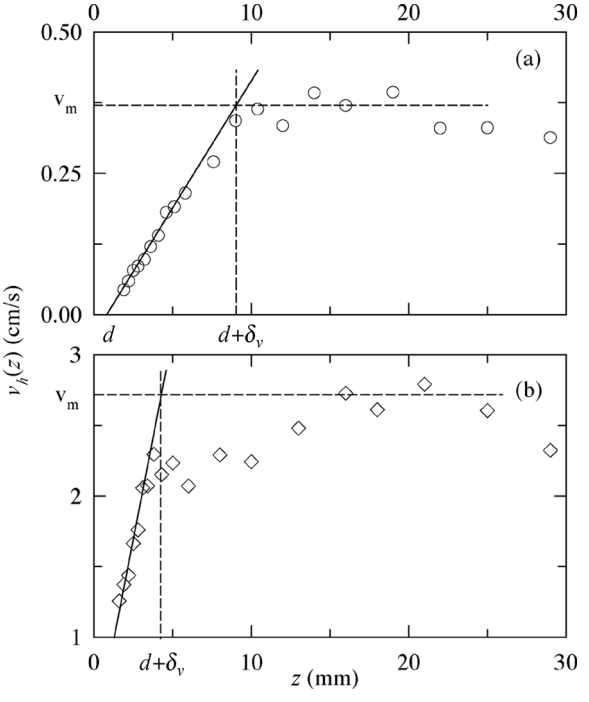

Figure 4. Time-averaged velocity profile $v_h(z)$ as a function of z in the $k = 8$ mm rough cell at (a) $Ra = 1.7 \times 10^8$ and (b) $Ra = 8.7 \times 10^9$. The solid lines are the linear fits to the small z data and the dashed lines indicate the maximum velocity v_m.

of the technique, v_v is found to be negligible. This situation is similar to that in the smooth cell, in which v_h is found to be the dominant velocity component near the conducting surface and its PDF is also Gaussian-like [13, 14, 17].

We now discuss the time-averaged velocity profile $v_h(z)$ as a function of distance z along the central vertical axis. Figure 4 shows the measured $v_h(z)$ at two different Rayleigh numbers in the rough cell with $k = 8$ mm. It is seen from figure 4(a) that the measured $v_h(z)$ increases linearly with z (solid line) when z is less than the roughness height k. As z is moved out of the groove region ($z > k$), $v_h(z)$ reaches a maximum value v_m (dashed line) and then decays to zero (not shown) when z is further increased towards the cell centre. The velocity profiles measured in the rough cell have a similar shape to those in the smooth cell [13, 17] but also show some interesting new features. First, the fitted linear function reaches zero at a finite value of $z = d$, indicating that the velocity profile very close to the bottom of the groove is no longer directly proportional to z. It appears that the entire velocity profile is shifted upward by a distance d, at which the velocity intersects the z-axis. Similar upward shift has been observed previously in turbulent shear flows over a rough wall and is referred as the mean height of momentum absorption by the surface [9, 18]. This upward shift can be explained simply by the fact that the horizontal shear flow is blocked partially by the rough elements on the surface, resulting in a stagnant layer of fluid deep inside the grooves. One would expect that such a sheltering effect becomes less effective at higher flow velocities, and indeed we find that the measured value of d decreases with increasing Ra. As will be shown below, the maximum velocity v_m near the rough surface increases with Ra.

With this understanding of d, we now can define the 'total boundary layer thickness', $d+\delta_v$, as a distance, at which the extrapolation of the linear part of $v_h(z)$ equals to the maximum

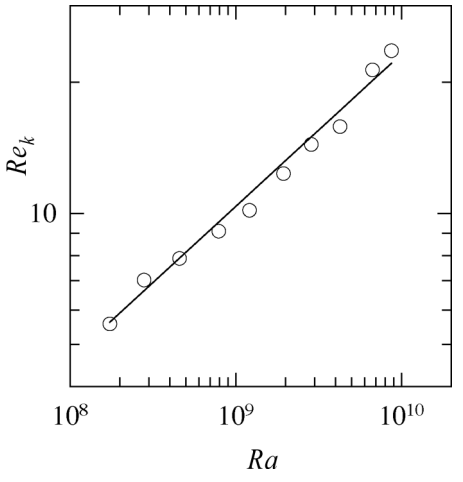

Figure 5. Measured roughness Reynolds number Re_k as a function of Ra in the rough cell with $k = 8$ mm. The solid line is the power law fit $Re_k = 7.34 \times 10^{-3} Ra^{0.35}$.

velocity v_m (see figure 4(a)). The slope of the linear function is the shear rate γ_v, so that $\gamma_v = v_m/\delta_v$. It is seen from figure 4(b) that the measured $v_h(z)$ at large Ra develops a shoulder region near $z \simeq k$. The time-averaged velocity in the shoulder region is approximately 20% smaller than the maximum velocity v_m (dashed line). The shoulder region is found in all the measured $v_h(z)$ when $Ra > 1 \times 10^9$. In this case, one can still define the total boundary layer thickness, $d + \delta_v$, in a way similar to that shown in figure 4(a) (see figure 4(b)).

To understand the shape change of the measured $v_h(z)$, we compute the roughness Reynolds number, $Re_k = u_* k/\nu$, which is the ratio of the roughness height k over the friction length ν/u_*. Here the friction velocity u_* is given by $u_* = (\nu\gamma_v)^{1/2}$ [6]. Figure 5 shows Re_k as a function of Ra obtained in the rough cell with $k = 8$ mm. It is seen that the measured Re_k varies from 5 to 23 in our working range of Ra and can be well described by a power law $Re_k = 7.34 \times 10^{-3} Ra^{0.35}$ (solid line). Previous experiments [19, 20] have shown that the effect of the surface roughness on the velocity boundary layer can be characterized by three different Re_k regimes. When $Re_k < 5$–10, the surface roughness does not affect the logarithmic velocity profile very much and the flow is 'dynamically smooth.' The flow becomes 'fully rough' when $Re_k > 40$. In the intermediate range of Re_k (5–10 $< Re_k <$ 40), the flow is considered 'transitionally rough.' In this case, the logarithmic velocity profile becomes dependent on parameters which characterize the spatial structure of the rough surface. It is seen from figure 5 that the convective flow in the $k = 8$ mm rough cell becomes 'transitionally rough' when $Ra > 1 \times 10^9$, above which we indeed find that the shape of the measured $v_h(z)$ is changed.

3.2 *Rayleigh-number dependence of the boundary layer properties*

We now examine the Ra-dependence of the three boundary layer properties: the maximum velocity v_m (the speed of the LSC), the shear rate γ_v, and the total boundary layer thickness $d + \delta_v$. Figure 6 shows the normalized maximum velocity $Pe = v_m L/\kappa$ (the Peclét number) as a function of Ra in the rough cells with $k = 8$ mm (triangles) and $k = 3$ mm (diamonds). The dashed line indicates the measured Pe ($v_m L/\kappa = 0.37 Ra^{0.5}$) by Xin *et al.* [13] in a smooth cell having the same geometry as that of the rough cells. It is seen that within the experimental uncertainties, the velocity data obtained in the rough cells overlap with those in the smooth cell.

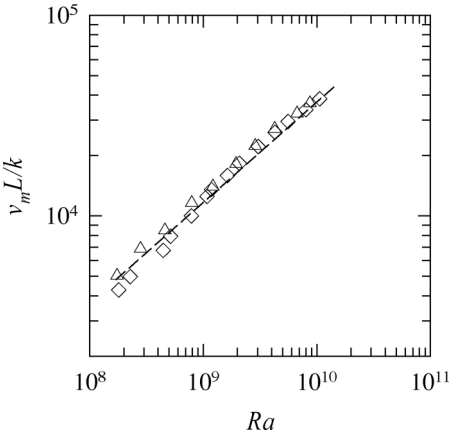

Figure 6. Normalized maximum velocity $v_m L/\kappa$ as a function of Ra in the rough cells with $k = 8$ mm (triangles) and $k = 3$ mm (diamonds). The dashed line indicates the measured $v_m L/\kappa$ in the smooth cell by Xin *et al.* [13].

From the velocity measurements near the lower rough surface, we find that the azimuthal orientation of the LSC is at an angle of 45° relative to the lines of grooves (i.e. the rotation plane of the LSC is along the diagonal direction of the lattice formed by the bases of the pyramids), when the cylindrical cell is levelled. Ciliberto *et al.* [21] have found that the azimuthal orientation of the LSC can be adjusted by slightly tilting the convection cell to break its cylindrical symmetry. It is shown that such a small tilt does not affect turbulent natural convection very much. In the above velocity measurements, we tilted the cell by a small angle (<1°) such that the direction of the measured v_m is along the lines of the parallel grooves (x-axis) from the lower side of the plate to the higher side of the plate. The incident laser beams are directed along a central groove perpendicular to the direction of the LSC. With this arrangement, we are able to measure the local velocity inside the valley of the grooves.

Figure 7 shows the normalized shear rate $\gamma_v L^2/\kappa$ as a function of Ra in the rough cells with $k = 8$ mm (triangles) and $k = 3$ mm (diamonds). The dashed line indicates the measured $\gamma_v L^2/\kappa$ ($= 0.74Ra^{0.66}$) in the smooth cell by Xin *et al.* [13]. It is seen that the measured shear

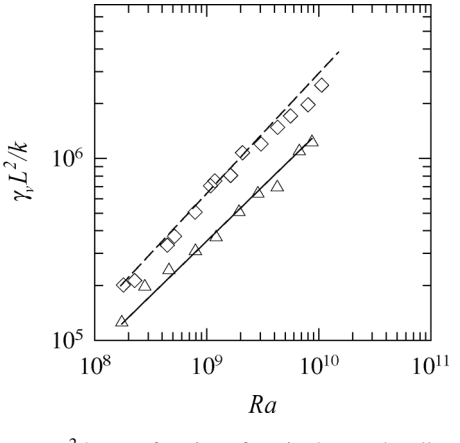

Figure 7. Normalized shear rate $\gamma_v L^2/\kappa$ as a function of Ra in the rough cells with $k = 8$ mm (triangles) and $k = 3$ mm (diamonds). The solid line shows the power-law fit, $\gamma_v L^2/\kappa = 1.4Ra^{0.6}$, to the $k = 8$ mm data. The dashed line indicates the measured $\gamma_v L^2/\kappa$ ($= 0.74Ra^{0.66}$) in the smooth cell by Xin *et al.* [13].

rate in the $k = 3$ mm rough cell is essentially the same as that in the smooth cell. The measured γ_v in the $k = 8$ mm rough cell is decreased by more than 45% at $Ra = 1 \times 10^9$, when compared with the smooth cell. The solid line in figure 7 shows the power-law fit, $\gamma_v L^2/\kappa = 1.4Ra^{0.6}$, to the $k = 8$ mm data. Because the maximum velocity v_m outside the viscous boundary layer (or equivalently $Pe = v_m L/\kappa$) is the same for both the rough and smooth cells, the decrease of the shear rate in the rough cell suggests that the surface roughness impedes the growth of velocity in the viscous boundary layer. Recent flow visualization by Du and Tong [2, 4] showed that the interaction between the horizontal shear flow due to the large-scale circulation and the rough surface creates a secondary flow (eddies) in the groove region. These eddies oppose the linear increase of the local velocity, because their vorticity is opposite to that of the large-scale circulation.

Figure 8(a) shows the measured δ_v as a function of Ra in the rough cells with $k = 8$ mm (triangles) and $k = 3$ mm (diamonds). The measured $\delta_v = 99Ra^{-0.16}$ mm [13] in the smooth cell (dashed line) is also shown for comparison. It is seen that the measured δ_v in the $k = 3$ mm rough cell is the same as that in the smooth cell for small values of Ra. At larger Ra ($>3 \times 10^9$), however, δ_v starts to level off. The measured δ_v in the $k = 8$ mm rough cell does

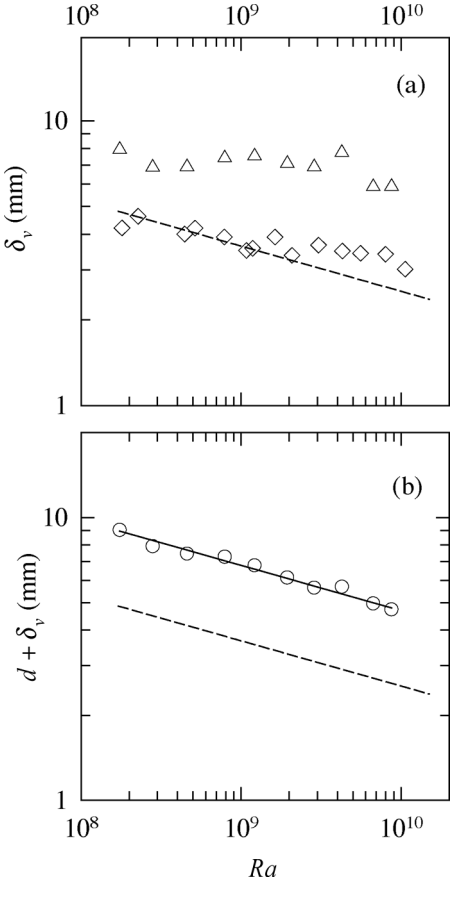

Figure 8. (a) Measured boundary layer thickness δ_v as a function of Ra in the rough cells with $k = 8$ mm (triangles) and $k = 3$ mm (diamonds). (b) Measured total boundary layer thickness $d + \delta_v$ as a function of Ra in the rough cell with $k = 8$ mm. The solid line represents the power-law fit $d + \delta_v = 187Ra^{-0.16}$ (mm). The dashed line in (a) and (b) indicates δ_v measured in the smooth cell $\delta_v = 10Ra^{-0.16}$ (cm) [13].

not change very much with increasing Ra and remains at a constant value very close to the roughness height k. Figure 8(b) shows the Ra-dependence of the total boundary layer thickness $d+\delta_v$ in the $k = 8$ mm cell. The solid line shows the power-law fit $d+\delta_v = 187Ra^{-0.16}$ (mm). Again, the dashed line represents $\delta_v = 99Ra^{-0.16}$ mm measured in the smooth cell [13]. It is seen that the scaling exponent for $d + \delta_v$ is the same as that for δ_v in the smooth cell, but the power-law amplitude is increased by a factor close to 2. In is also seen from figure 8(a) that $\delta_v \simeq k$ for both the 3 and 8 mm roughness cells. This can be understood from the fact that the origin of the vertical coordinate z is at the base of the pyramid (see figure 1) and δ_v essentially measures this displacement.

It should be mentioned that the classification of dynamically smooth, transitional and fully rough flows discussed in section 3.1 is based on the roughness effect on the logarithmic velocity profile, which is located further away from the rough surface. It is shown in figures 7 and 8 that the flow close to and within the roughness is influenced strongly by the surface roughness even under the 'dynamically smooth' condition (low Re_k or Ra). We not that at the lowest Ra ($\simeq 2\times 10^8$) of the experiment, the roughness height k ($= 8$ mm) is still approximately five times larger than the friction length ν/u_* (see figure 5). The requirement for the viscous sublayer near the boundary not being affected by the surface roughness should be $k < \nu/u_*$ (or $Re_k < 1$) [22]. This is a stronger condition than the 'dynamically smooth' condition ($Re_k < 5$–10) for the logarithmic velocity profile.

To further characterize the state of convective motion, we measure the global heat transport in the rough cell. The normalized heat flux across the cell is expressed by the Nusselt number $Nu = PL/(\pi R^2 \kappa \Delta T)$, where P is the total heating power, ΔT is the resulting temperature difference across the fluid layer of thickness L, and πR^2 is the cross-sectional area of the cell. Figure 9 shows the measured Nu as a function of Ra in the rough cells with $k = 8$ mm (solid circles) and $k = 3$ mm (open circles). The solid line represents a power-law fit to the 8 mm data: $Nu = 0.67\ Ra^{0.35}$ and the dashed line to the 3 mm data: $Nu = 0.54\ Ra^{0.35}$. For comparison, the dash-dotted line shows $Nu = 0.19\ Ra^{0.28}$ which was measured by Lui and Xia in a smooth cell of the same dimension and at similarly values of Pr [23]. It is seen that heat transport in the rough cells is increased considerably when compared to the smooth case. The amount of increase in the heat flux varies with the roughness height k. The measured

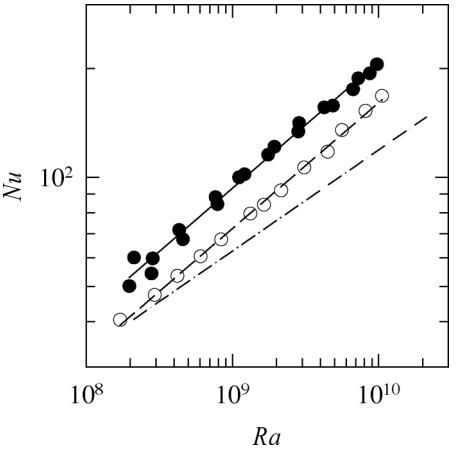

Figure 9. Measured Nusselt number Nu as a function of Ra in the rough cells with $k = 8$ mm (solid circles) and $k = 3$ mm (open circles). The solid and dashed lines represent power-law fits to the respective data: $Nu = 0.67Ra^{0.35}$ ($k = 8$ mm) and $Nu = 0.54Ra^{0.35}$ ($k = 3$ mm). The dash-dotted line represents $Nu = 0.19Ra^{0.28}$ which is measured in a smooth cell of the same dimension and at similar Pr [23].

$Nu(Ra)$ in the $k = 8$ mm cell is $\sim$30% larger than that in the $k = 3$ mm cell. These findings agree qualitatively with the previous heat transport measurements in rough cells [1, 2, 4], i.e. surface roughness enhances heat transfer. However, the power-law exponents for the rough cells in the present experiment increased significantly as compared to the smooth case, which is more close to 2/7 for comparable values of Ra and Pr and obtained in cells of similar design (other than roughness) [13, 14, 23, 25, 26]. Previous heat transport measurements by Shen *et al.* and by Du and Tong [1, 2, 4] reported that the power-law exponents for the smooth and rough cells are approximately the same. We note that the constructions of the rough cells used in the two experiments are somewhat different. The rough surfaces used in the present experiment are machined directly on thick copper plates. In the previous experiments by Shen *et al.* and by Du and Tong, the rough surfaces were machined on two separate brass plates and then attached to the upper and lower smooth substrates that were also made of brass.

It has been shown [2, 4] that the time-averaged surface temperature at the tip differs from that at the bottom of the groove. Thus, unlike the smooth case, the rough surface is no longer isothermal under uniform heating. The non-uniform boundary layer dynamics could be sensitive to the small construction differences mentioned above. For example, the surface temperature difference between the tip and groove could be affected by the thermal diffusion time, $\sim k^2/\kappa$, between the tip and groove over the solid plate. So the thermal properties of the pate material will be important, we note that the thermal conductivity of brass is $\sim$1/3 of copper. While the rough brass plates used in the experiments reported in [1, 2, 4] were in good thermal contact with the substrates, small contact resistance may influence the lateral surface inhomogeneity. Further measurements of $Nu(Ra)$ over a wider range of Ra are certainly needed in order to resolve the above difference.

It should be mentioned that Ciliberto and Laroche (CL) [3] also found a change in the scaling exponent of Nu with Ra. However, the situation is somewhat different. As reported by CL, when the surface roughness was in the form of a regular pattern like in the present case they found no change in the scaling exponent and only when the roughness pattern was made to be random did they find a change in the exponent. It should also be mentioned that CL observed a decrease in the value of Nu in their rough cell (as compared to the smooth case), instead of an enhancement observed in our experiment. This may be due to the fact that their surface roughness was created by gluing glass spheres onto the bottom copper plate and glass has a much lower thermal conductivity than copper. Thus it appears that the exponent change in the two cases may arise from different mechanisms.

4. Conclusion

We have carried out a systematic study of the velocity boundary layer over a rough conducting surface in turbulent natural convection. The experiment is conducted in a convection cell having rough upper and lower surfaces and filled with water. The technique of dual-beam cross-correlation spectroscopy is used to measure the time-averaged velocity profile $v_h(z)$ as a function of distance z along the central vertical axis of the cell. The velocity measurements in the rough cell are compared with those in the smooth cell. It is found that the viscous boundary layer near the rough surface can be characterized by three quantities: the maximum velocity v_m, the shear rate γ_v and the total boundary layer thickness $d + \delta_v$. These three quantities are found to obey power laws of Ra.

The maximum velocity v_m is located outside the rough surface and represents the speed of the large-scale circulation. The measured v_m as a function of Ra remains unchanged when compared with that in the smooth cell. The Ra-dependence of the viscous boundary layer thickness $d + \delta_v$ is found to be the same as that in the smooth cell, but the power-law amplitude

is increased by a factor close to 2. The velocity boundary layer near the rough surface is shifted upward by a distance d, because the horizontal shear flow is blocked partially by the rough elements on the surface, resulting in a stagnant layer of fluid deep inside the grooves. The interaction between the horizontal shear flow and the rough surface creates small eddies in the groove region. These eddies oppose the linear increase of the local velocity, and therefore the measured shear rate γ_v is reduced considerably in the groove region. The experiment reveals that the effect of the surface roughness to the velocity boundary layer is confined mainly in the groove region, whereas the large-scale flow outside the rough surface is not affected very much by the surface roughness. It is also found that the magnitude and the scaling exponent of the measured Nusselt number are both larger than those in the smooth case.

Acknowledgements

We gratefully acknowledge the Research Grants Council of Hong Kong SAR for support of this work under grant no. CUHK 403003. Tong is supported by the Research Grants Council of Hong Kong SAR under grant no. HKUST 603003.

References

[1] Shen, Y., Tong, P. and Xia, K.-Q., 1996, *Physical Review Letters*, **76**, 908.
[2] Du, Y.-B. and Tong, P., 1998, *Physical Review Letters*, **81**, 987.
[3] Ciliberto, S. and Laroche, C., 1999, *Physical Review Letters*, **82**, 3998.
[4] Du, Y.-B. and Tong, P., 2000, *Journal of Fluid Mechanics*, **407**, 57.
[5] Villermaux, E., 1998, *Physical Review Letters*, **81**, 4859.
[6] Siggia, E.D., 1994, *Annual Review of Fluid Mechanics*, **26**, 137.
[7] Zocchi, G., Moses, E. and Libchaber, A., 1990, *Physica A*, **166**, 387.
[8] Xi, H.-D., Lam, S. and Xia, K.-Q., 2004, *Journal of Fluid Mechanics*, **503**, 47.
[9] Raupach, M. R., Antonia, R. A. and Rajagopalan, S., 1991, *Applied Mechanics Review*, **44**, 1.
[10] Qiu, X.-L. and Xia, K.-Q., 1998, *Physical Review E*, **58**, 486.
[11] Xia, K.-Q., Xin, Y.-B. and Tong, P., 1995, *Journal of the Optical Society of America*, **12**, 1571.
[12] Tong, P. and Xia, K.-Q., 1998, In R. J. Donnelly and K. R. Sreenivasan, (Eds) *Flow at Ultra-High Reynolds and Rayleigh Numbers* (New York: Springer-Verlag).
[13] Xin, Y.-B., Xia, K.-Q. and Tong, P., 1996, *Physical Review Letters*, **77**, 1266.
[14] Xin, Y.-B. and Xia, K.-Q., 1997, *Physical Review E*, **56**, 3010.
[15] Lam, S., Shang, X.-D., Zhou, S.-Q. and Xia, K.-Q., 2002, *Physical Review E*, **65**, 066306.
[16] Landau, L. D. and Lifshitz, E. M., 1987, *Fluid Mechanics*, (Oxford: Pergamon Press).
[17] Qiu, X.-L., Yao, S.-H. and Tong, P., 2000, *Physical Review E*, **61**, R6075.
[18] Jackson, P.S., 1981, *Journal of Fluid Mechanics*, **111**, 15.
[19] Ligrani, P. M. and Moffat, R. J., 1986. *Journal of Fluid Mechanics*, **162**, 69.
[20] Bandyopadhyay, P. R., 1987, *Journal of Fluid Mechanics*, **180**, 231.
[21] Ciliberto, S., Cioni, S. and Laroche, C., 1996, *Physical Review E*, **54**, R5901.
[22] Monin, A.S. and Yaglom, A.M., 1971, *Statistical Fluid Mechanics* (Cambridge, MA: MIT Press)
[23] Lui, S.-L. and Xia, K.-Q., 1998, *Physical Review E*, **57**, 5494.
[24] Belmonte, A., Tilgner, A. and Libchaber, A., 1995, *Physical Review E*, **50**, 269.
[25] Xia, K.-Q. and Qiu, X.-L., 1999, *Europhysics Letters*, **46**, 171.
[26] Xia, K.-Q., Lam, S. and Zhou, S.-Q., 2002, *Physical Review Letters*, **88**, 064501.
[27] Heslot, F., Castaing, B. and Libchaber, A., 1987, *Physical Review A*, **36**, 5870.